Simulation and Analysis of Aerodynamic Characteristics of High-Altitude Long-Distance Gliding UUV (Unmanned Underwater Vehicle)

Huan-huan Liu, Guang Pan, and Xiao-xu Du

Abstract In order to study the aerodynamic characteristics of the high-altitude long-distance gliding UUV, Sects. 2, 3 and 4 states the process of the analysis and research mentioned in the title, whose core consists of: "Under the environment of FULENT, defining the boundary conditions, meshing, solving the Navier–Stokes equations, completes the three-dimensional flow field numerical simulation of UUV under the condition of subsonic (Sect. 3). The longitudinal aerodynamic characteristics, lateral aerodynamic characteristics and the characteristics of the manipulation derivation properties are analyzed in Sect. 4." The simulation results, given in Figs. 3, 4, 5 and 6, show that the aerodynamic characteristics meet the requirements of the low draft characteristics of the aircraft and the static stability. Not only mentioned can conducive the next step of the manipulation of the aircraft, stability and ballistic characteristics, but also provide an important basis to further improve the design and model processing test.

Keywords Aerodynamic characteristics • Modeling and simulation • UUV

1 Introduction

The technology of high-altitude long-distance gliding UUV is an integration of high-altitude volplane and underwater voyage (Wu Wenhui et al. 2009; Zhu Xinyao et al. 2011). The UUV is launched by carrier aircraft at an altitude of 10,000 m,

H. Liu (✉) • G. Pan • X. Du
School of Marine Engineering, Northwestern Polytechnical University, Xi'an 710072, China
e-mail: Shirley.3251@163.com

and after the safe separation, the UUV relies on the automatically bounced hang gliding device gliding in the air hundreds of kilometers to reach the pre-attack region, and then variants (hang gliding device leaves the UUV) into water quickly, completing the scheduled tasks. The aerodynamic characteristic plays an important part in the gliding performance of high-altitude long-distance gliding UUV. The good aerodynamic characteristic is the main indicator of the design of aerodynamic configuration. And the accurate of the fluid dynamic parameters not only reflect the properties of the design of aerodynamic configuration, but have an important role in further research of stability and manipulation properties. In the issue, under the environment of FULENT, solving the Navier–Stokes equations, completes the three-dimensional flow field numerical simulation of UUV under the condition of subsonic. Analyzing the longitudinal aerodynamic characteristics, lateral aerodynamic characteristics and the characteristics of the manipulation derivation properties; the results show that the aerodynamic characteristics meet the requirements of the low draft characteristics of the aircraft and the static stability. Not only mentioned can conducive the next step of the manipulation of the aircraft, stability and ballistic characteristics, but also provide an important basis to further improve the design and model processing test.

2 Aerodynamic Configuration of the High-Altitude Long-Distance Gliding UUV

On the basis of existing UUV, installing a set of wings which have the function of high-altitude gliding and guidance, the high-altitude long-distance gliding UUV in is completed (Li Xin-guo and Fang Qun 2005; Qian Xing-fang et al. 2008), including gliding-wing (NACA64A2-215), even tail (NACA0012-64), vertical tail, control system and UUV, overall layout scheme is shown in Fig. 1.
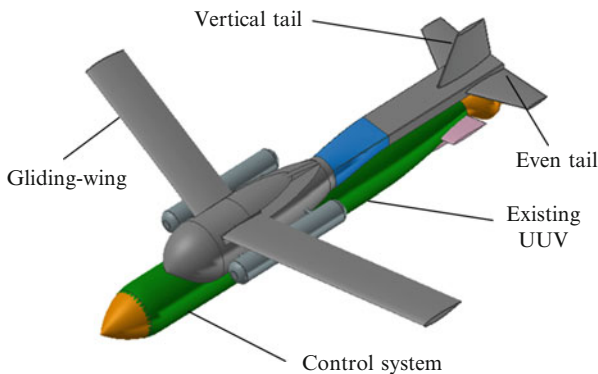

Fig. 1 Overall layout of the high-altitude long-distance gliding UUV

3 Numerical Simulation Method of the High-Altitude Long-Distance Gliding UUV

3.1 Mesh

Due to the high requirement on the computer to generate the three-dimensional meshes, and the complexity characteristic of the UUV caused the workload of the mesh is huge and extremely difficult (Singh et al. 1995). Therefore, unstructured grids is selected to discrete the UUV spatially when generates meshes, because of the less workload, besides, the unstructured grids have a strong adaptability of complex shape and the results in the accuracy range. The three-dimensional assembly model is imported into the environment of ICEM by the intermediate form. Setting the control parameters, adjusting the local density constantly to make sure the grid density appropriate and the calculation is not too much (Mavriplis and Jameson 1990; Qunzhen and Massey 1999). Figure 2 shows the unstructured mesh of the UUV.

The flow field area 10 times the model length, about 5.0 million mesh.

3.2 Control Equation

3.2.1 Mathematical Model

In the flow motion, continuity equation is also known as conservation of mass, and the general conservation differential form is expressed as follows (Zhang Zhaoshun
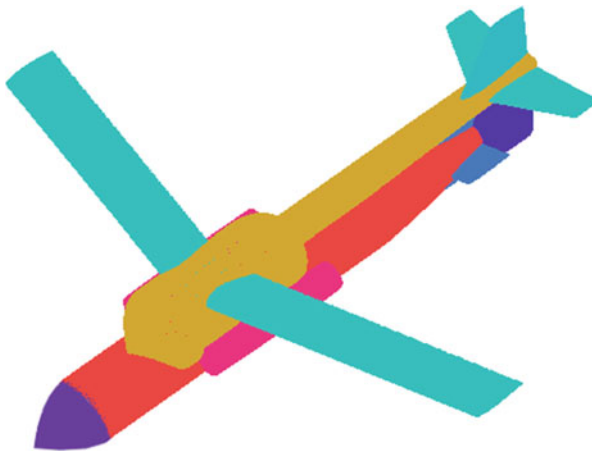

Fig. 2 Meshes on the surface of the UUV

and Cui Guixiang 2006; Dongjoo Kim and Haecheon Choi 2000; Zhang and Wang 2004; Mavriplis et al. 1989):

$$\frac{\partial \rho}{\partial t} + \frac{\partial}{\partial x_i}(\rho u_i) = S_m \tag{1}$$

Where, S_m is the mass added into the continuous phase.

The momentum equation is expressed as follows in the inertial coordinate system:

$$\frac{\partial \rho}{\partial t}(\rho u_i) + \frac{\partial}{\partial x_j}(\rho u_i u_j)$$

$$= -\frac{\partial p}{\partial x_i} + \frac{\partial \tau_{ij}}{\partial x_j} + \rho g_i + F_i \tag{2}$$

Where, P is static pressure, τ_{ij} is stress tensor, which would be expressed: $\tau_{ij} = [\mu(\partial u_i/\partial x_j + \partial u_j/\partial x_i)] - 2/3(\delta_{ij}\mu u_l/x_l)$, g_i and F_i are gravity volume force and external volume force respectively.

Energy conservation equation is expressed as follows

$$\frac{\partial}{\partial t}\left[\rho\left(e + \frac{U^2}{2}\right)\right] + div\left[\rho(e + \frac{U^2}{2})\vec{U}\right]$$

$$= \rho\vec{f} \cdot \vec{U} + \nabla \cdot (\lambda \nabla T) + \rho\dot{q} + \nabla \cdot \left(\vec{U} \cdot T_{ij}\vec{e_i}\vec{e_j}\right) \tag{3}$$

Turbulent kinetic k energy equation

$$\frac{\partial(\rho k)}{\partial t} + \frac{\partial(\rho k u_i)}{\partial x_i}$$

$$= \frac{\partial}{\partial x_j}\left(\Gamma_k \frac{\partial k}{\partial x_j}\right) + G_k + \rho\varepsilon \tag{4}$$

Dissipation rate $k - \varepsilon$ equation:

$$\rho\frac{D\varepsilon}{Dt} = \frac{\partial}{\partial x_j}\left[\left(\mu + \frac{\mu t}{\sigma\varepsilon}\right)\frac{\partial\varepsilon}{\partial x_j}\right] + \rho c_1 S\varepsilon$$

$$- \rho c_2 \frac{\varepsilon^2}{k + \sqrt{v\varepsilon}} + c_{1\varepsilon}\frac{\varepsilon}{k}c_{3\varepsilon}G_b \tag{5}$$

3.2.2   Boundary Condition

1. Boundary no-slip condition
   In the steady flow around a fixed object, the speed on the surface: $\overrightarrow{U}_b = 0$. The no-slip condition on the surface is as follows:

$$\overrightarrow{U} = 0 \tag{6}$$

2. Thermal equilibrium condition of the temperature of solid surface
   The temperature of the fluid particles should be the same with the local surface temperature:

$$T_w = T_b \tag{7}$$

3. The condition of kinematics, dynamics and thermodynamics of the fluid boundary surface
   On the boundary surface of the non-invasive fluid, if the surface tension is neglected, then at any point of the interface on both sides, the velocity, pressure and temperature should be equal. That is:

$$\overrightarrow{U}_+ = \overrightarrow{U}_-, \overrightarrow{P}_+ = \overrightarrow{P}_-, T_+ = T_- \tag{8}$$

## 3.3   Batch Processing of Multiple Loading Conditions and Working Condition Setting

Considering the diversity of the working condition to simulate the UUV, including the variable attack angle and variable sideslip angle, besides, under the environment of FLUENT, several attack angles and sideslip angles can not be set one time. Therefore, with the help of user-defined function UDF provided by FLUENT (Ji Bing-bing and Chen Jin-ping 2012; Wang Fan and Huang Peng 2008), completes the numerical simulation in FULETN environment. The speed of the flow is 0.7 Ma, and the Reynolds number Re is 6.33×10^6.

4   Analysis of Aerodynamic Characteristics of High-Altitude Long-Distance Gliding UUV

4.1   Analysis of Longitudinal Characteristics

Figure 3 reflects the longitudinal characteristic curve of the UUV. And sideslip angle $\beta = 0°$, no rudder angles.

Fig. 3 Longitudinal
characteristic curve of the
UUV (**a**) lift coefficient curve
(**b**) drag coefficient curve (**c**)
Pitching moment coefficient
curve
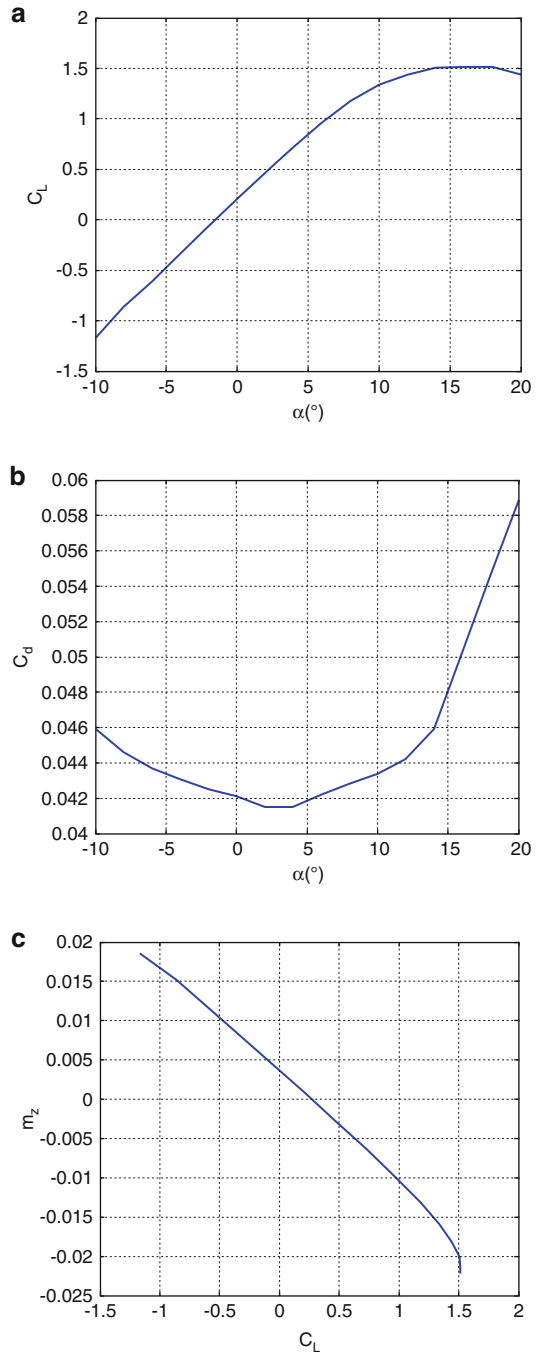
Sub-figure (a) shows the lift coefficient C_L curve. From the figure we can conclude that the lift coefficient performances linear feature when the attack angle in the range of $-5° \sim 10°$. Whereas with the increase of attack angle, the lift coefficient of nonlinear gradually obvious, showing the increase first and then downward trend. It is because with the increase of attack angle, the airflow around the gliding-wing and even tail gradually separated, and the flow changed into turbulence. We can also conclude that the UUV attack angle is $-1.66°$ when life force equals zero, and the maximum lift coefficient is 1.5 and attack angle equals 15°. And C_L^{α} equal 0.11/°.

Sub-figure shows the drag coefficient C_d curve. From the figure we can conclude that when the attack angle is in the range of $-6° \sim 6°$, the drag coefficient is very small, about 0.04. The UUV performances low-resistance characteristic, and meeting the design requirements. But with the increase of attack angle, the incident flow area of the UUV increases, and airflow separates, caused the drag coefficient increases significantly.

Sub-figure (c) shows the relationship between pitching moment coefficient m_z and lift coefficient C_L. A significant linear relationship can be seen from the figure. And the derivative dm_z/dC_L is -0.016. Zero lift pitching moment coefficient is 0.0039.

4.2 Analysis of Lateral Characteristics

Figure 4 shows the lateral characteristics curves of the UUV. And attack angle $\alpha = 0°$, no rudder angles.

From the Fig. 4, we can see that lateral force coefficient, yawing moment coefficient and roll moment coefficient show the anti symmetric characteristic as to β. And $C_z^{\beta} = -0.210/°$, $m_y^{\beta} = -0.0040/°$, $m_x^{\beta} = -0.0024/°$ meets the lateral static stability conditions: $C_z^{\beta} < 0$, $m_y^{\beta} < 0$, $m_x^{\beta} < 0$, satisfying the design requirement (Li Weiji 2005).
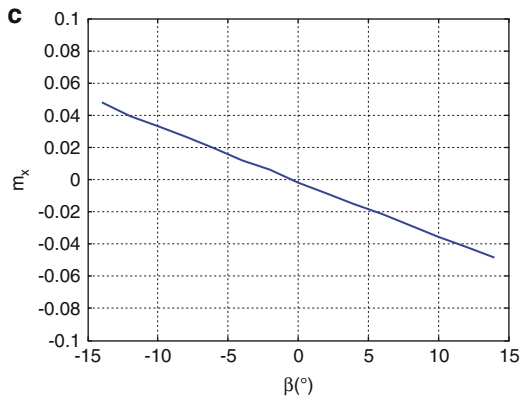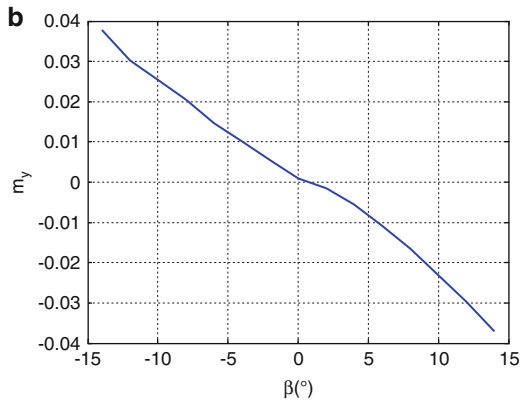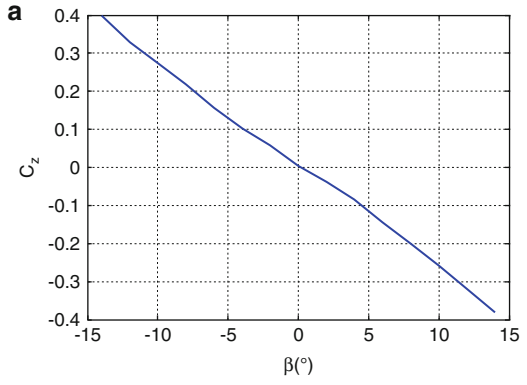
4.3 Analysis of Manipulation Derivation Properties

4.3.1 Derivative of the Horizontal Tail Manipulation

Figure 5 shows the manipulation derivation curves caused by even tail. And attack angle $\alpha = 0°$, sideslip angle $\beta = 0°$, vertical rudder angle $\delta_v = 0°$.

From the Sub-figure (a), we can see that when the horizontal rudder in the range of $-5° \sim 5°$, the lift coefficient approximately shows linear characteristic, and $C_L^{\delta_h}$ is 0.0117/°. Besides, while horizontal rudder equals 0, C_L is about 0.91. That is, the

Fig. 4 Lateral characteristics curves of the UUV (**a**) Lateral coefficient curve (**b**) Yawing moment coefficient curve (**c**) Roll moment coefficient curve
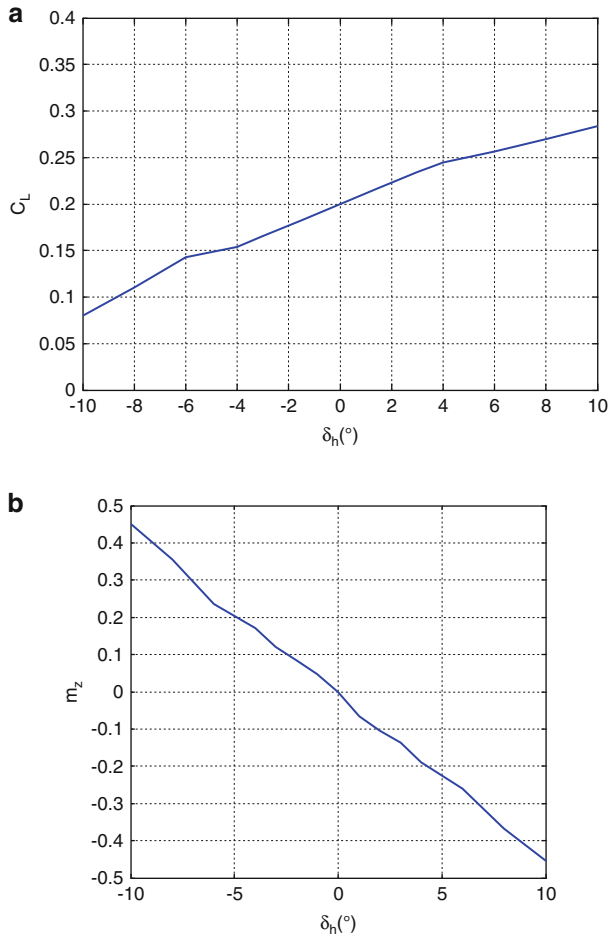
Fig. 5 manipulation derivation curves caused by even tail (**a**) Lift coefficient curve (**b**) Pitching moment coefficient curve

lift coefficient is about 0.2 in cruise condition, meet the design need. However, with the δ_h increases, airflow separates, non-linear becomes clear, but the overall trend is horizontal ruder increases, lift coefficient increases.

From the Sub-figure (b), we can see that when the horizontal rudder in the range of $-10° \sim 10°$, the pitching moment coefficient shows linear characteristic, and $m_z^{\delta_h}$ is $-0.0512/°$, satisfying the design requirement.

4.3.2 Derivative of the Vertical Tail Manipulation

Figure 6 shows the manipulation derivation curves caused by vertical tail. And attack angle $\alpha = 0°$, sideslip angle $\beta = 0°$, horizontal rudder angle $\delta_h = 0°$.

From the Sub-figure (a), we can see that when the vertical rudder in the range of $-10° \sim 10°$, the lateral force coefficient shows linear characteristic, and $C_z^{\delta_v}$ is 0.0090/°.

From the Sub-figure (b), we can see that when the vertical rudder in the range of $-5° \sim 5°$, the yawing moment coefficient is approximately linear, and $m_y^{\delta_v}$ is 0.0045/°. But with the vertical rudder increases, the non-linear characteristic becomes clear. And the yawing moment increase gradually while the efficiency of vertical tail decreases.

From the Sub-figure (c), we can see that when the vertical rudder in the range of $-5° \sim 5°$, the roll moment coefficient shows linear characteristic, and $m_x^{\delta_v}$ is 0.0011/°. But with the vertical rudder increases, the non-linear characteristic becomes clear.

It should be noted that the yawing moment coefficient derivative is bigger the capacity of the vertical tail changing course and the efficiency of the tail is higher. Besides, with the vertical rudder increases, the efficiency of vertical tail decreases. The bigger of the lateral force coefficient derivative $C_z^{\delta_v}$ and roll moment derivative $m_x^{\delta_v}$, the worse of the UUV's flight. By moving down the gravity center, adjusts the roll moment coefficient derivative $m_x^{\delta_v}$ to counteract the impact of $m_x^{\delta_v}$ on the UUV, making sure the $m_x^{\delta_v} < 0$, and meets the static stability feature. The only way to reduce the lateral force coefficient is to reduce the vertical tail area and increase the vertical tail arm, but it can not be eliminated. All statements above, provides a guideline for the future to further improve the design.

5   Conclusion

It can be seen from the above simulation results and analysis. Under the environment of FULENT, solving the Navier–Stokes equations, completes the three-dimensional flow field numerical simulation of UUV under the condition of subsonic. Analyzing the longitudinal aerodynamic characteristics, lateral aerodynamic characteristics and the characteristics of the manipulation derivation properties; the results show that the aerodynamic characteristics meet the requirements of the low draft characteristics of the aircraft and the static stability. Not only mentioned can conducive the next step of the manipulation of the aircraft, stability and ballistic characteristics, but also provide an important basis to further improve the design and model processing test.

Fig. 6 manipulation derivation curves caused by vertical tail (**a**) Lateral force coefficient curve (**b**) Yawing moment coefficient curve (**c**) Roll moment coefficient curve
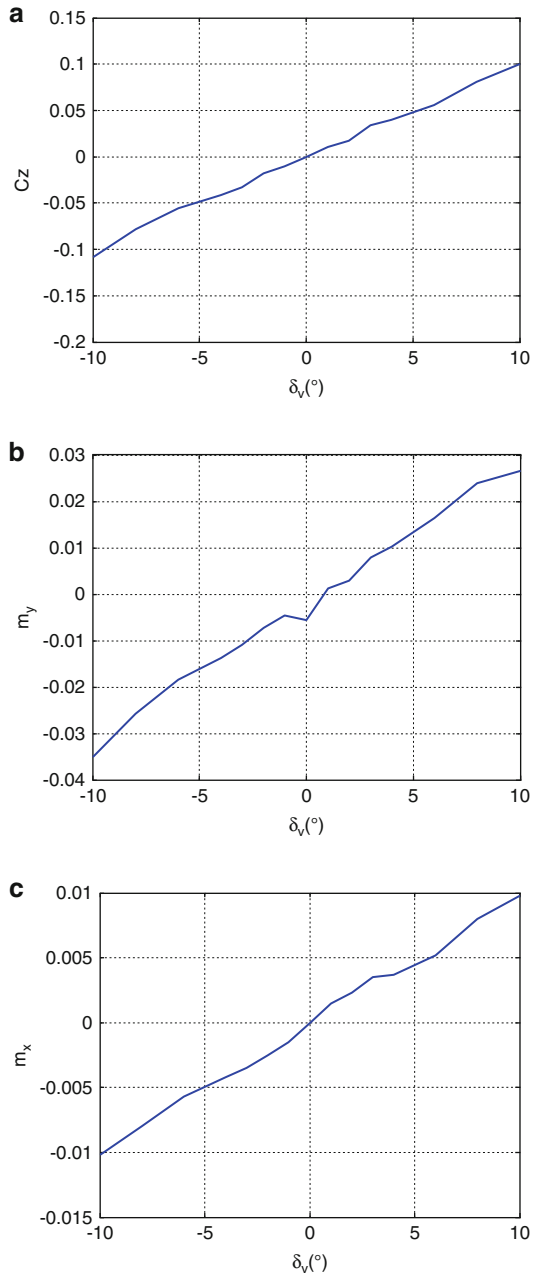
References

Dongjoo Kim, Haecheon Choi (2000) A second-order time-accurate finite volume method for unsteady incompressible flow on hybrid unstructured grids. J Comput Phys 162:411–428

Ji Bing-bing, Chen Jin-ping (2012) ANSYS ICEM CFD grid partitioning technique example explanation [M]. China Water Power Press, Beijing, pp 58–65

Li Weiji (2005) Aircraft design [M]. Northwestern Polytechnical University Press, Xi'an, pp 145–149

Li Xin-guo, Fang Qun (2005) Winged missile flight dynamics [M]. Northwest Industry University Press, Xi'an

Mavriplis DJ, Jameson A (1990) Multigrid solution of the Navier-Stokes equations on triangular meshes. AIAA J 28(8):1415–1425

Mavriplis DJ, Jamson A, Martinelli L (1989) Multigrid solution of the Navier–Stokes equations on triangular meshes. In: 27th AIAA aerospace sciences meeting and exhibit, pp 89–0194

Qian Xing-fang, Lin Rui-xiong, Zhao Ya-nan (2008) Missile flight mechanics [M]. Beijing Institute of Technology Press, Beijing, pp 28–48

Qunzhen Wang, Massey SJ (1999) Solving Navier–Stokes equations with advanced turbulence models on three-dimensional unstructured grids. In: 37th AIAA aerospace sciences meeting and exhibit, Reno, Nevada, 11–14 January 1999, paper 99–0156

Singh KP, Newman JC, Baysal O (1995) Dynamic unstructured method for flows past multiple objects in relative motion. AIAA J 33(4):641–649

Wang Fan, Huang Peng (2008) Senior fluent application and example analysis [M]. TsingHua University Press, Beijing, pp 279–314 (in Chinese)

Wu Wenhui, Pan Guang, Mao Zhaoyong et al (2009) Key technology about the simulation for the trajectory of upper airspace long-distance gliding UUV [J]. Torpedo Technol 17(4):10–15

Zhang Zhaoshun, Cui Guixiang (2006) Fluid mechanics [M]. TsingHua University Press, Beijing, pp 69–82

Zhang LP, Wang ZJ (2004) A block LU-SGS implicit dual time-stepping algorithm for hybrid dynamic meshes. Comput Fluid 33:891–916

Zhu Xinyao, Song Baowei, Mao Zhaoyong et al (2011) Aerodynamic parameters calculation and aerodynamic characteristics analysis of high-altitude gliding UUV [J]. Comput Simul 28(5):179–183